Magn Reson Med Sci 2023; 22; 27–43
doi:10.2463/mrms.rev.2021-0118 Published Online: March 23, 2022

REVIEW

Arterial Spin Labeling for Pediatric Central Nervous System Diseases: Techniques and Clinical Applications

Mika Kitajima[1*] and Hiroyuki Uetani[2]

Dynamic susceptibility contrast (DSC) and arterial spin labeling (ASL) are techniques used to evaluate brain perfusion using MRI. DSC requires dynamic image acquisition with a rapid administration of gadolinium-based contrast agent. In contrast, ASL obtains brain perfusion information using magnetically labeled blood water as an endogenous tracer. For the evaluation of brain perfusion in pediatric neurological diseases, ASL has a significant advantage compared to DSC, CT, and single-photon emission CT/positron emission tomography because of the lack of radiation exposure and contrast agent administration. However, in ASL, optimization of several parameters, including the type of labeling, image acquisition, background suppression, and postlabeling delay, is required, because they have a significant effect on the quantification of cerebral blood flow (CBF).

In this article, we first review recent technical developments of ASL and age-dependent physiological characteristics in pediatric brain perfusion. We then review the clinical implementation of ASL in pediatric neurological diseases, including vascular diseases, brain tumors, acute encephalopathy with biphasic seizure and late reduced diffusion (AESD), and migraine. In moyamoya disease, ASL can be used for brain perfusion and vessel assessment in pre- and post-treatment. In arteriovenous malformations, ASL is sensitive to detect small degrees of shunt. Furthermore, in vascular diseases, the implementation of ASL-based time-resolved MR angiography is described. In neoplasms, ASL-derived CBF has a high diagnostic accuracy for differentiation between low- and high-grade pediatric brain tumors. In AESD and migraine, ASL may allow for accurate early diagnosis and provide pathophysiological information.

Keywords: *acute encephalopathy with biphasic seizure and late reduced diffusion, arterial spin labeling, migraine, pediatric neuroimaging, vascular disease*

Introduction

Arterial spin labeling (ASL) is based on the use of blood as an endogenous tracer by employing spatially selective labeling of the inflowing blood that inverts its longitudinal magnetization. After an appropriate delay time, a rapid readout imaging is used to obtain the tissue magnetization. By subtraction of an image obtained after labeling from an image that is identical to the label condition, except for the absence of inversion of inflowing blood, an image of the labeled blood that has reached the brain tissue is obtained.[1–3] ASL is repeatable with no use of a gadolinium-based contrast agent (GBCA) and enables calculation of absolute cerebral blood flow (CBF). No use of GBCA and ionizing radiation exposure are the advantages of repeated MR examinations in clinical situations, particularly in pediatric patients and patients with contraindications to GBCA, including allergy and renal or liver failure. In addition, repeated administration of GBCA causes its deposition in the brain.[4,5] Furthermore, peripheral intravenous catheterization of GBCA administration may not be feasible in children.

The technical improvement of pulse sequences, including labeling, background suppression, and readout, and the increasing availability of 3-T MR imagers have led to the rapid widespread clinical use of ASL. Recent technical advances in ASL have improved the image quality and accuracy of quantification metrics.[6,7] Moreover, time-efficient acquisition of dynamic ASL images provides hemodynamic information, such as digital subtraction angiography (DSA) data.[8–17] In ASL, optimization of parameters and understanding of the techniques used are

[1]Department of Medical Imaging Sciences, Faculty of Life Sciences, Kumamoto University, Kumamoto, Kumamoto, Japan
[2]Diagnostic Radiology, Faculty of Life Sciences, Kumamoto University, Kumamoto, Kumamoto, Japan

*Corresponding author: 4-24-1, Kuhonji, Chuo-ku, Kumamoto, Kumamoto 862-0976, Japan. Phone: +81-373-5483, Fax: +81-373-5519, E-mail: mkitaji@kumamoto-u.ac.jp

Received: August 31, 2021 | Accepted: January 12, 2022

required. Furthermore, radiologists should understand the pathophysiology of perfusion in various neurological diseases for the utilization of ASL in clinical practice.

In this article, we review the basic and recently developed ASL techniques, as well as the pitfalls in pediatric neuroimaging. We then conduct a literature review and illustrate our cases in several relatively common pediatric neurological diseases in which ASL provides useful brain perfusion information.

Technical Aspects of ASL

In 2015, Alsop et al. published a consensus statement on the practical implementation of ASL in clinical practice.[18] As a standard approach, pseudo-continuous labeling, background suppression, segmented three-dimensional readout without vascular crushing gradients, and calculation and presentation of both label and control difference images and CBF in absolute units using a simplified model are recommended. Regarding the labeling method, pseudo-continuous ASL (pCASL) uses a narrow labeling plane and a train of very short RF pulses plus a gradient pulse. It offers high efficiency of labeling and induces a higher SNR and reproducibility than does pulsed ASL (PASL).[19] In addition, pCASL can significantly reduce specific absorption rate in comparison with continuous ASL (CASL) which induces the high tissue energy deposition and requires high duty cycle. Vascular suppression is useful to eliminate the intra-arterial signals from total ASL signals; however, it decreases SNR and may remove important clinical information, such as the presence of delayed flow and arteriovenous shunting. Therefore, the use of vascular crushing gradients is not recommended in clinical practice.

Postlabeling delay (PLD), the time between the end of labeling and signal acquisition, is one of the critical factors that yield accurate perfusion information in ASL; it relates to the mean arterial transit time (ATT), which is the time taken for labeled blood to flow from the labeling region to the tissue compartment. The PLD must be long enough to allow labeled protons to flow into the imaging slice but not so long that the majority of measurable tracers have decayed. Ideally, the PLD is set within this range and just after the longest ATT in a given patient. When the PLD is shorter than the ATT, the labeled protons that have not reached the brain tissue can be recognized as arterial signals known as ATT artifact (Fig. 1). This finding confounds the accurate measurement of CBF; however, it indicates the slow flow rate through the stenosis or the prolongation of the time for labeled blood to arrive via collateral pathways.[3,20,21] The surrounding low signal intensity reflects more distal parenchyma that the labeled blood has not yet arrived at the time of signal acquisition. Because the ATT is required for the quantification of CBF, its accurate measurement is of great importance. Thus, ASL with multiple different PLDs (multi-delay ASL) has been proposed

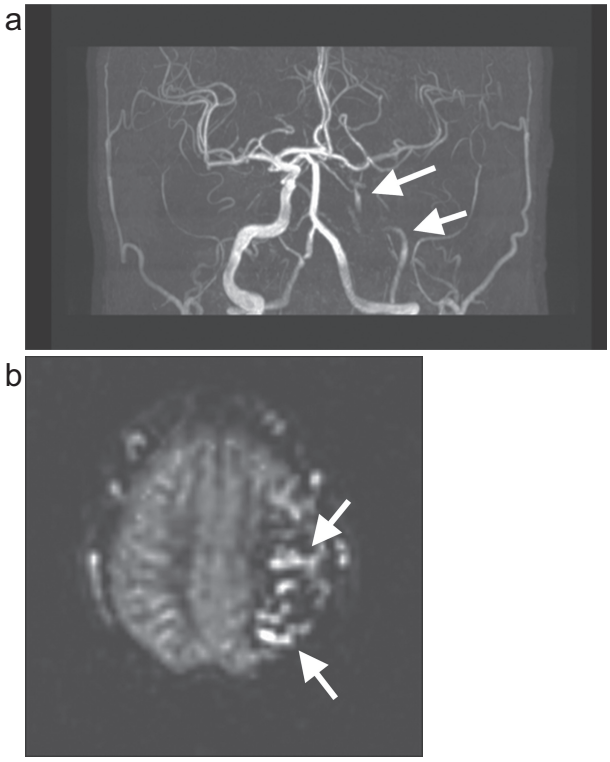

Fig. 1 A 57-year-old man with the left internal carotid artery stenosis. A TOF-MRA (**a**) shows a severe stenosis of the left internal carotid artery (arrows). An ASL perfusion image obtained using 3D pCASL with the labeling duration of 1800 ms and the PLD of 2000 ms (**b**) shows a mix of high and low ASL signal intensity indicating arterial transit artifact in the left middle arterial territory. Multiple hyperintense signal bands (arrows) indicate the presence of the labeled blood in the arteries, and the surrounding low signal intensity reflects the parenchyma that the labeled blood has not reached at the time of imaging. pCASL, pseudo-continuous arterial spin labeling; PLD, postlabeling delay; TOF, time-of-flight.

to overcome the issue of the ATT (Fig. 2). Whole-brain ASL perfusion images at each PLD, CBF map, and bolus arrival time (BAT) map of Fig.2 are shown in Supplementary Fig. 1. However, multi-delay ASL typically extends the imaging time and degrades the sensitivity of the resulting perfusion images. Recent technical advances in multi-delay ASL, such as time-encoded ASL, can shorten the imaging time and decrease the adverse effects of the ATT.[6,7,22] There are several challenges for the accurate quantification of CBF using ASL, and CBF measured using ASL shows a strong correlation with that measured using ^{15}O-H_2O positron emission tomography (PET).[23]

One of the diversifications of ASL technology is the time-efficient acquisition of ASL images, yielding time-resolved MR angiography (MRA). Several ASL-based time-resolved MRA techniques have been developed, and the clinical implementation of these techniques has been reported (Fig. 3). Current vessel-encoded and super-selective pCASL methodologies have been applied for flow-territory

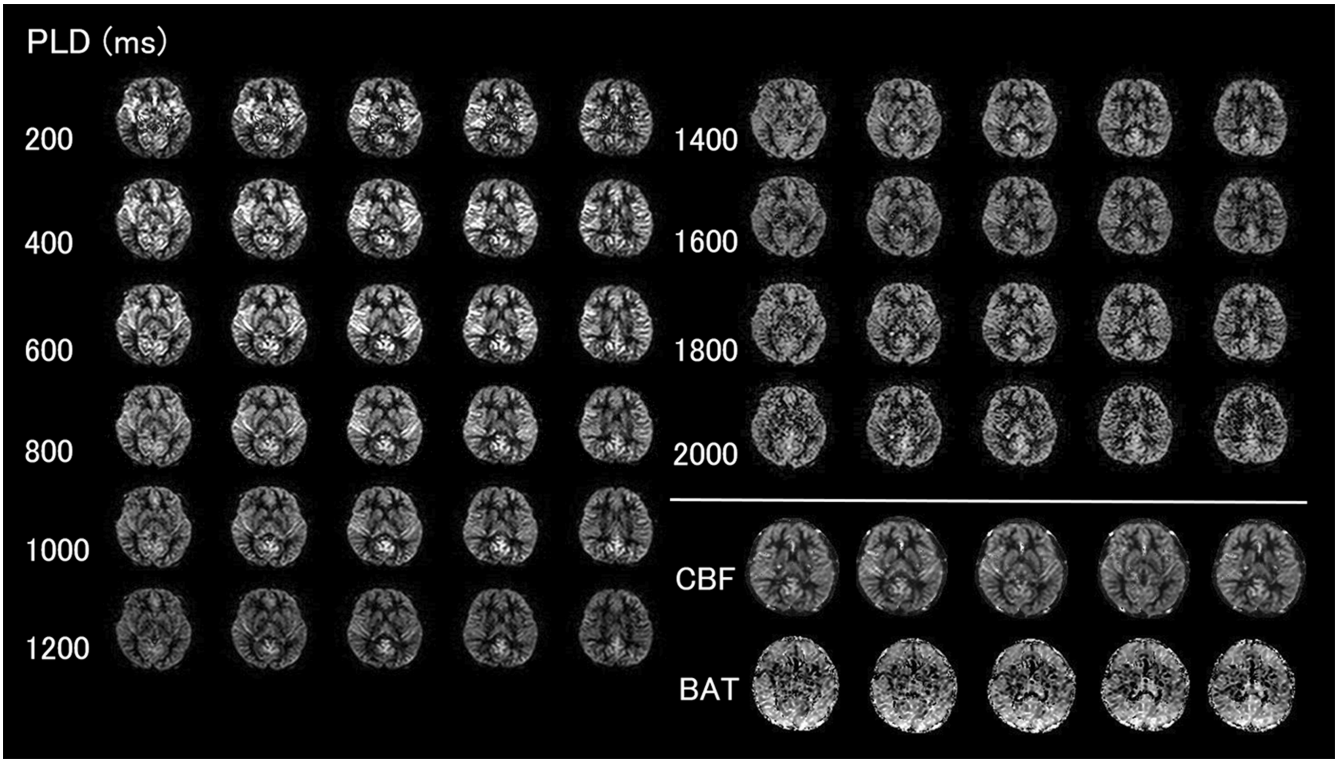

Fig. 2 An example of multi-delay ASL perfusion images at different PLDs of 200, 400, 600, 800, 1000, 1200, 1400, 1600, 1800, and 2000 ms, CBF map, and BAT map of an 8-year-old girl. The ASL images were obtained using 3D pCASL without vascular crusher, and the readout sequence was GRASE. BAT, bolus arrival time; CBF, cerebral blood flow; GRASE, gradient- and spin-echo; pCASL, pseudo-continuous arterial spin labeling; PLD, postlabeling delay.

mapping methods, and they can provide blood flow information that is highly similar to DSA. Furthermore, combined 4D angiography and perfusion imaging has been reported.[9–13]

Physiological Factors Related to ASL in the Pediatric Population

When interpreting ASL images, the age dependence of PLD and CBF should be considered. An appropriate PLD is determined considering several factors, including patient age, hemodynamics, brain regions of interest, and the disease process. The recommended PLD is 2000 ms in neonates, 1500 ms in children, 1800 msec in healthy subjects < 70 years of age, and 2000 ms in adult clinical patients or healthy subjects > 70 years of age assessment in ASL.[18] Another study of healthy young and elderly volunteers reported that the limits of agreement were too wide for quantitative ASL to be considered satisfactorily accurate, with systematic overestimation of CBF in young subjects and underestimation in elderly subjects.[24]

Quantitative CBF values vary depending on the study population, imaging sequence, and mathematical modeling, with approximate ranges as follows: neonates, 5–30 mL/100 g/min; infants, 30–70 mL/100 g/min; children, 80–120 mL/100 g/min; teenagers, 60–100 mL/100 g/min; adult 40–80 mL/100 g/min; and elderly, 30–60 mL/100 g/min.[25–27] A study addressed the correlation of ASL-derived gray matter CBF and ADC with age in children aged 4 months to 18 years and found that gray matter CBF increased with age, except for the globus pallidus and that the ADC of all structures decreased with age. The most rapid changes in ADC occurred prior to the age of 5 years.[28] Unlike ADC changes, CBF increased with age, with decreased variability at older ages. Another report of age-dependent ASL-derived CBF change showed a nonlinear trajectory of CBF change in children younger than 3 years.[29] In ASL of pediatric patients, a consistent pattern of increased signal-to-noise ratio and globally elevated absolute CBF has been observed compared with that of adults.[30] This globally increased signal intensity due to higher baseline CBF, more rapid mean transit time, increased baseline magnetization values in the gray and white matters, and increased T1 values in the blood and tissue.[30] Decreased susceptibility artifacts at the base of the skull from immature paranasal sinus development may also play a role in improving image quality.[30]

Sedation and anesthetic drugs also have variable effects on CBF. Inhalational narcotics and ketamine cause

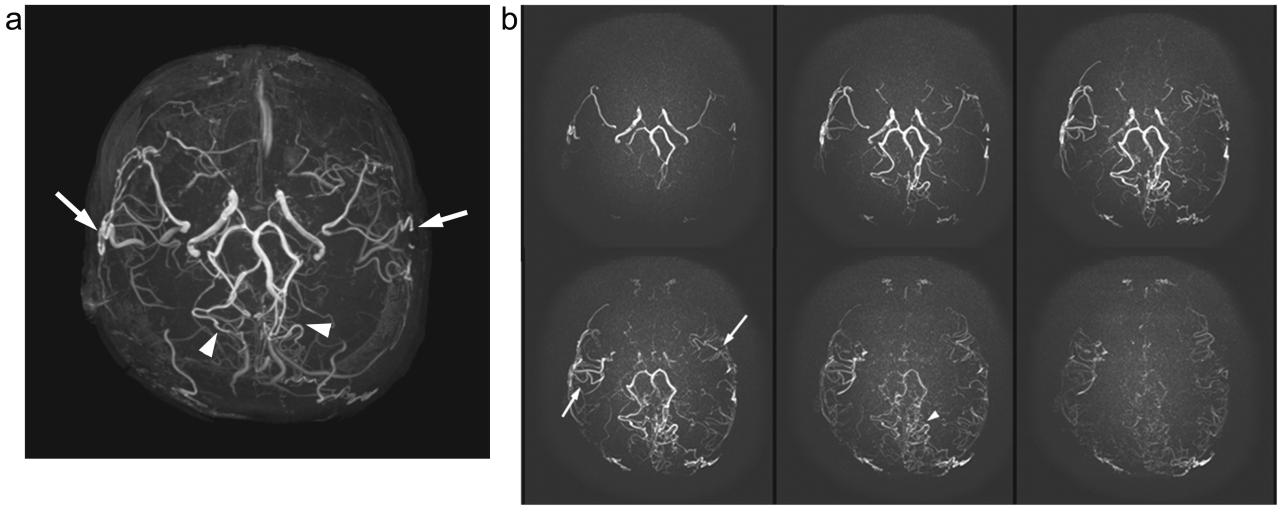

Fig. 3 An 11-year-old girl who underwent bilateral vascular repair for moyamoya disease. A TOF-MRA image (**a**) shows the occlusive change of the bilateral middle cerebral arteries and the bilateral bypassed arteries (arrows) connecting to the distal site of the bilateral middle cerebral arteries. Collaterals from the posterior cerebral arteries (arrowheads) are also observed. Additionally, ASL-based time-resolved MRA using signal targeting with alternating radio frequency with the asymmetric inversion slabs (mASTAR) technique images (**b**) successfully visualize that the labeled arterial blood of the bypass arteries is flowing into the bilateral distal middle cerebral arteries retrogradely (arrows). Collaterals (**b**) (arrowheads) are also observed. Temporal resolution of ASL-based time-resolved MRA is about 200 ms. ASL, arterial spin labeling; mASTAR, multiple TI MRA with ASTAR (signal targeting alternating radiofrequency using asymmetric inversion slab); MRA, MR angiography; TOF, time-of-flight.

vasodilation with increased CBF, while intravenous narcotics decrease CBF.[25] By contrast, a recent study of 100 healthy children aged 4 months to 18 years reported no significant CBF differences in any brain regions between sedated children via intravenous propofol administration and non-sedated children.[28] Other physiological factors, including hyper- or hypocapnia, hormonal status, circadian rhythm, nutrition, and hydration, affect CBF.[25]

Vascular Diseases

Moyamoya disease (Table 1)

Moyamoya disease is the most common pediatric cerebrovascular disease in East Asia. It causes stenosis and occlusion of the terminal segment of the internal carotid artery and results in the development of compensatory collateral circulation paths called moyamoya blood vessels.[31] The main role of neuroimaging in moyamoya disease is to identify the parenchyma in which collateral pathways are inadequate to maintain sufficient oxygen delivery, extent of stenosis and collateral circulation, and presence of infarcts, and brain atrophy. Traditionally, the extent of stenosis and collateral circulation is assessed using DSA, which is the gold standard for moyamoya disease staging.

ASL can provide information regarding hemodynamic impairment but is complicated by the long blood arrival times in moyamoya disease, which can manifest as either signal voids or hyperintense signals, depending on the imaging parameters.[32] This drawback induces inaccurate CBF measurements using ASL. In a comparative study using simultaneously acquired single- and multi-delay ASL and [^{15}O]-water PET, multi-delay ASL did not perform differently from [^{15}O]-water PET in detecting perfusion abnormalities[33]; however, single-delay ASL significantly overestimated the extent of hypoperfusion in patients with moyamoya disease. In addition, long PLDs (4000 ms, compared with PLD of 2500 ms) are needed to achieve good correlations for relative CBF between PET and ASL. In contrast, Fahlström et al. evaluated the effect of ATT artifacts on ASL-derived CBF obtained using single-dealy PLD with and without acetazolamide challenge in patients with moyamoya disease and found that ATT artifacts have negligible overestimation effects on the calculated vascular region-based CBF.[34] Qiu et al. compared CBF measured by xenon CT as a reference with that measured by MRI including multi-delay pCASL, velocity-selective ASL, and DSC in 10 moyamoya disease patients and found that CBF measured by velocity-selective ASL had the least dependence of the error on transit delay caused by slow flow.[35]

The oxygen extraction fraction (OEF) is another important hemodynamic parameter in brain perfusion and may serve as a biomarker for tissue health. It increases in patients with moyamoya disease, when the extent of collateralization and/or autoregulation is insufficient to maintain adequate oxygen delivery to the tissue. Hara et al. compared the visual assessment using a four-point grading system for ASL images obtained with two different PLDs (1525 ms and 2525 ms)

Table 1 ASL for moyamoya disease

Evaluation	ASL findings	ASL technique	Assessment	Gold standard	Ref no.
CBF	Multi-delay pCASL can detect hypoperfusion area comparable to [^{15}O]-water PET, but single-dealy ASL overestimated the extent of hypoperfusion.	Single- and multi-delay pCASL (3.0T)	aCBF	[^{15}O]-water PET	33
	ATT artifacts in single-delay ASL is negligible in CBF overestimation effects.	Single-delay pCASL (3.0T)	CBF	CBF measured by ASL with ATT artifact	34
	Velocity-selective ASL with less sensitivity for slow flow is suitable than pCASL for accurate measurement of CBF.	Velocity-selective ASL (3.0T)	CBF	Xenon CT	35
OEF	Low perfusion detected by ASL using a long PLD has a high specificity for elevated OEF.	Multi-delay pCASL (3.0T)	Visual assessment	[^{15}O]-gas PET	36
CR	CR at pre- and post-revascularization state can be assessed by ASL with acetazolamide challenge.	Single-delay pCASL (1.5T)	rCBF	^{99}mTc-HMPAO-SPECT	37
Postoperative collateral circulation	Agreement for collateral grading and anastomosis patency between ASL and DSA was moderate to good.	Single-delay pCASL (1.5T or 3.0T)	Visual assessment	DSA	38
Distal and collateral vessels	Time-resolved ASL-based MRA enables better visualization of distal arteries and collaterals with higher CNR compared with CINEMA.	pCASL with keyhole and view sharing (3.0T)	Visual assessment& CNR	DSA	9
	AccASL improves the visualization of distal cerebral arteries and collaterals than TOF-MRA.	AccASL (3.0T)	Visual assessment& CNR	DSA	14
	Time-resolved super-selective ASL-based MRA is better than 3D TOF-MRA for visualization of collaterals after bypass surgery and has high consistency with DSA.	Super-selective pCASL (3.0T)	Visual assessment	DSA	12
Revascularization territory	Superselective ASL precisely depicts the revascularization territory.	Super-selective pCASL (3.0T)	Visual assessment	DSA	15
Hyper-perfusion syndrome	Hyperperfusion syndrome can be detected as an increase of perfusion more than 100% compared to the pre-operative perfusion with very high sensitivity and moderate specificity.	Single-delay pCASL (1.5T)	rCBF	Clinical symptoms	39

aCBF, absolute cerebral blood flow; AccASL, acceleration-selective arterial spin labeling; CINEMA, contrast inherent inflow-enhanced multiphase angiography; CNR, contrast-to-noise ratio; CR, cerebrovascular reactivity; DSA, digital subtraction angiography; MRA, MR angiography; rCBF, relative cerebral blood flow; TOF, time-of-flight.

and OEF obtained from ^{15}O gas PET in patients with moyamoya disease.[36] Their results showed that the low score on ASL, indicating hypoperfusion, correlated with the increase of OEF. The visual assessment using ASL with a long PLD of 2525 ms had the highest specificity (98.5%) for elevated OEF.

Before surgical vascular repairs in patients with moyamoya disease, cerebrovascular reserve capacity is usually assessed by single-photon emission CT (SPECT) with intravenous administration of acetazolamide. Yun et al. evaluated the diagnostic accuracy of ASL to depict impaired cerebrovascular reactivity using acetazolamide administration by comparing the cerebrovascular reactivity index concordance between ASL and SPECT in patients with moyamoya disease.[37] They found that ASL has excellent performance in the identification of impaired cerebrovascular reactivity, and the area under the receiver operating characteristic curve for ASL in the detection of impaired cerebrovascular reactivity was at least 0.85.

In moyamoya disease, the assessment of collateral circulation and brain perfusion before and after vascular repair is important. Lee et al. evaluated the patency of the bypass arteries and collateral blood flow between ASL and DSA.[38] They defined the bright signal intensity relative to the cortical signal intensity as poor patency of the bypass arteries and found that the agreements for collateral grading and anastomosis patency between ASL and DSA were moderate to good. Furthermore, several studies showed the usefulness of superselective ASL imaging for the patients with

Table 2 ASL for AVM

Evaluation	ASL findings	ASL technique	Gold standard	Ref no.
Detection of AVM	The venous ASL signal is the strong predictor of positive findings on DSA in detection of small (< 2 cm) AVMs.	Single-delay pCASL (1.5T)	DSA	41
Degree of arteriovenous shunting	AVM signal intensity on ASL correlated well with the degree of AV shunting.	Single-delay pCASL (3.0T)	DSA	47
Delineation of nidus	Combined use of 4D ASL and 4D CE-MRA provides sufficient spatio-temporal angiographic information for delineation of AVM niduses.	Multi-delay PASL (3.0T)	DSA	48
Feeding arteries and venous drainage	AccASL better visualizes AVMs with high CNR compared with TOF-MRA.	AccASL (3.0T)	DSA	16
	4D-S-PACK can delineate hemodynamics in AVMs with high sensitivity and specificity in identification of feeding arteries and venous drainage.	ss-pCASL with keyhole and view-sharing (3.0T)	DSA	17
Assessment of AVMs after treatment	ASL can detect the perfusion change within nidus and steal phenomena after gamma knife therapy for AVMs.	Single-delay PASL (3.0T or 1.5T)	DSA	50
	Nidal CBF measured by ASL may enable objective monitoring of AVM obliteration after radiosurgery or partial embolization.	Single-delay pCASL (1.5T)	DSA	51
	Combination of ASL and TOF-MRA is superior to gadolinium-enhanced MR imaging in detecting residual small AVMs (< 20 mm) after radiosurgery.	Single-delay pCASL (3.0T)	DSA	53
	ASL has high sensitivity (100%) and specificity (95%) in detection of residual AVMs following stereotactic radiosurgery as an abnormal venous ASL signal.	Single-delay pCASL (1.5T or 3.0T)	DSA	54

4D-S-PACK, 4D MR angiography based on super-selective pseudo-continuous arterial spin labeling with contrast inherent inflow-enhanced multiphase angiography-keyhole and view-sharing; ASL, arterial spin labeling; AVM, arteriovenous malformation; CE-MRA, contrast-enhanced MR angiography; DSA, digital subtraction angiography; ss-pCASL, super-selective pseudo-continuous arterial spin labeling.

moyamoya disease before and after bypass surgery.[12,15] Superselective ASL imaging precisely depicted the revascularization territory and vascular territory changes after bypass surgery in patients with moyamoya disease.[15]

ASL-based time-resolved MRA enables not only visualization of collateral vessels but also obtainment of dynamic flow information (Fig. 3). Togao et al. proposed a new ASL-based time-resolved MRA technique for better visualization of distal collateral vessels in patients with moyamoya disease.[9] It employs pCASL for better visualization of distal collateral vessels and the keyhole and view sharing technique for improving temporal resolution. This technique improves visualization and yields higher contrast-to-noise ratios (CNRs) in the distal cerebral arteries and leptomeningeal anastomosis collaterals with a very long transit time compared with contrast inherent inflow-enhanced multiphase angiography (CINEMA).[9] Wang et al. compared the visibility of bypass patency and intracranial collaterals between ASL-based time-resolved MRA which employed super-selective pCASL in conjunction with the keyhole and view sharing technique and time-of-flight (TOF)-MRA in patients who underwent bypass surgery for extra-intracranial vascular occlusion disease.[12] The visibility of bypass patency and intracranial collaterals was better in super-selective ASL-based time-resolved MRA than in 3D TOF-MRA. In addition, the visualization of intracranial collateral vessels on super-selective ASL-based time-resolved MRA was highly consistent with that obtained in DSA. As another ASL-based MRA for better visualization of distal collateral vessels, the acceleration-selective ASL (AccASL) has been introduced.[14] By employing an acceleration-dependent preparation which dephases spins that are accelerating or decelerating, AccASL can selectively image the arteries, without contamination from venous signal.[7] Togao et al. compared the visualization of vessels including collateral vessels and CNRs between TOF-MRA and AccASL in patients with moyamoya disease and showed that AccASL MRA yields

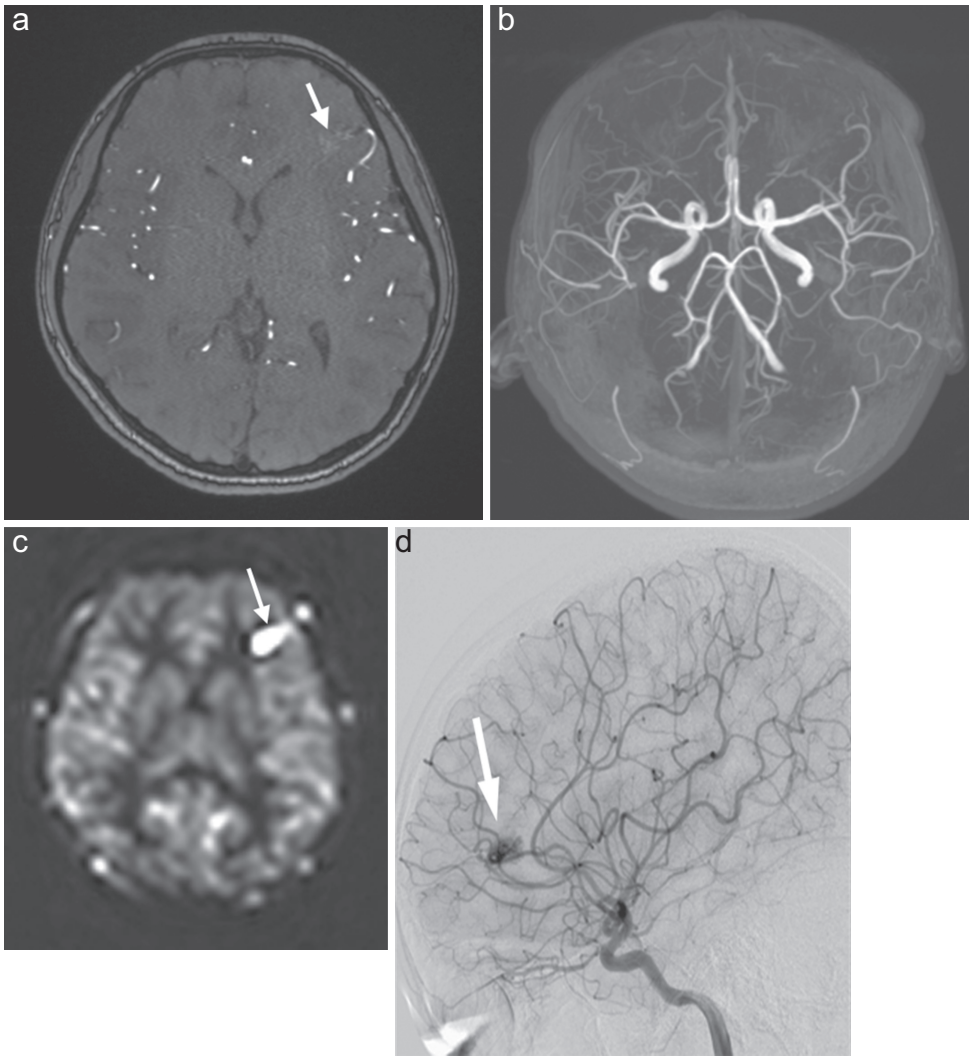

Fig. 4 An 11-year-old girl with a small AVM in the left frontal lobe. A source image of TOF-MRA (**a**) shows a faint abnormal high signal intensity (arrow) corresponding to the nidus in the left frontal lobe, whereas identification of the nidus is difficult on the MIP image (**b**). An ASL perfusion image (**c**) shows the "venous signal" (arrow) indicating AVM in the left frontal lobe. A DSA image of the left internal carotid artery (**d**) exhibits the small nidus (arrow) in the left frontal lobe. ASL, arterial spin labeling; AVM, arteriovenous malformation; DSA, digital subtraction angiography; MIP, maximum intensity projection; MRA, MR angiography; TOF, time-of-flight.

better visualization of distal cerebral arteries and collateral vessels than does TOF-MRA.[14]

During the early postoperative period of bypass surgery in patients with moyamoya disease, cerebral hyperperfusion syndrome can occur, as reperfusion is established in chronically ischemic cerebral territories. Agarwal et al.[39] reported that ASL provided high sensitivity (47%–100%) and specificity (45%–88%) for the detection of cerebral hyperperfusion.

Vascular malformation (Table 2)

Vascular malformations are defects of normal vascular morphogenesis that can involve capillary, venous, arterial, and/or lymphatic vessels. Cerebral arteriovenous malformations (AVMs) are high-flow malformations characterized by an abnormal nidus of vessels connecting the arterial and venous systems. The incidence of pediatric AVMs is estimated to represent 3% of all AVMs, and they tend to rupture more frequently than adult AVMs.[40] The number and origin of feeding arteries, as well as the degree of shunting and vascular steal from the brain parenchyma, determine the clinical severity. ASL can identify AVMs non-invasively as a venous ASL signal.[41] A venous ASL signal is caused by labeled protons bypassing the normal capillary bed, remaining intraluminal without tissue exchange, and entering the venous system before the signal has decayed. Even small malformations (< 2 cm) that may be missed on conventional sequences can be identified on ASL (Fig. 4).[41] In AVM cases with slow or rapid shunting lesions, multi-delay ASL may be useful. The surrounding brain parenchyma may demonstrate hypoperfusion due to arterial steal and impaired capillary exchange.[42]

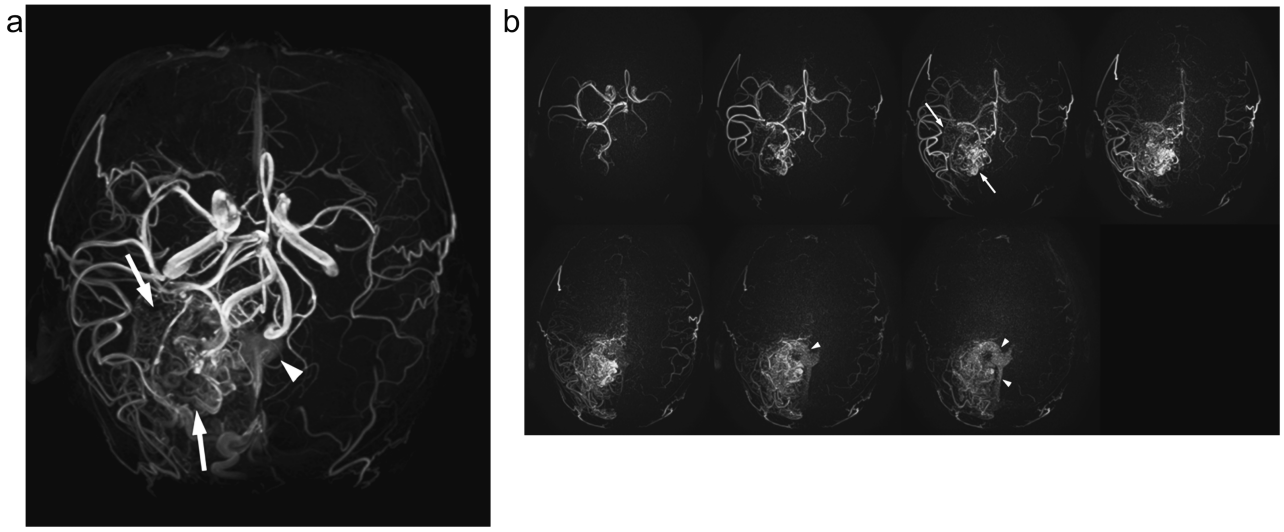

Fig. 5 An 18-year-old man with AVM in the right occipital lobe. A TOF-MRA MIP image (**a**) shows the nidus (arrows) fed by the right posterior cerebral artery mainly and the main draining vein (arrowhead). ASL-based time-resolved MRA using mASTAR technique images (**b**) successfully visualize that the labeled arterial blood of right posterior cerebral artery is flowing into the nidus (arrows). Subsequently, the vein of Galen and the straight sinus (arrowheads) are opacified (**b**). Temporal resolution of ASL-based time-resolved MRA is about 200 ms. ASL, arterial spin labeling; AVM, arteriovenous malformation; DSA, digital subtraction angiography; mASTAR, multiple TI MRA with ASTAR (signal targeting alternating radiofrequency using asymmetric inversion slab); MIP, maximum intensity projection; MRA, MR angiography; TOF, time-of-flight.

Multimodality therapies for AVMs are currently available, including resection, radiosurgery, and endovascular embolization. Complete angiographic obliteration of AVMs is required in the pediatric population, given their longer life expectancy and higher risk of rupture than adults.[40,43] Traditionally, DSA is performed to evaluate accurate size of the nidus, feeding arteries, and draining veins before treatment of AVMs, whereas the value of MRA in nidus delineation has been investigated.[44–46] When TOF-MRA is used solely for nidus delineation, the lack of hemodynamic information might lead to inclusion of the feeding arteries and draining veins in the nidus definitions.[44] This results in the overestimation or displacement of the centers of the nidus volumes.[45,46] Sunwoo et al.[47] used ASL to evaluate the degree of arteriovenous shunting within the AVM nidus and demonstrated that the AVM signal intensity on ASL correlated well with the degree of early vein opacification on DSA, which corresponds to the degree of arteriovenous shunting. The AVM signal intensity also demonstrated a positive relationship with the AVM size. Ozyurt et al.[48] tested whether the combined use of time-resolved ASL (4D ASL) and contrast-enhanced MR angiography (4D CE-MRA) can work as a prospective alternative to DSA for the delineation of the nidus in stereotactic radiosurgery (SRS) planning. The reproducibility of the target volumes with high agreement levels is achievable without using DSA, and the ASL technique provides sufficient spatiotemporal angiographic information for the delineation of AVM niduses.

For the accurate identification of the feeding arteries, vessel selectivity is necessary. Recently, ASL techniques for better visualization of AVM and its hemodynamic information have been reported (Fig. 5).[13,16,17] Togao et al. evaluated a new ASL technique, 4D MRA based on super-selective pCASL with contrast-enhanced timing-robust angiography-keyhole and view-sharing technique and its utility for the assessment of hemodynamics in AVMs.[17] They found that their ASL-based time-resolved MRA showed good vessel selectivity: the sensitivity and specificity for the identification of the feeding arteries were 100%, and those for the identification of venous drainage were more than 90%.

After treatment of AVMs, careful follow-up imaging is required, because AVMs progress over a period of 2–3 years.[49] Previous studies have demonstrated the utility of ASL in the evaluation of cerebral AVMs after treatment.[50–54] Leclerc et al. compared the detectability of residual AVMs after SRS between non-contrast MRI consisting of TOF-MRA plus ASL and contrast-enhanced MRI including contrast-enhanced dynamic MRA plus post-contrast thin-slice 3D T1-weighted image (T1WI).[53] The non-contrast enhancement method was superior to the contrast-enhanced methods for the detection of residual AVMs. Heit et al. compared the detection rate of residual AVMs between DSA and ASL and found that ASL was highly sensitive and specific in the detection of residual cerebral AVMs following SRS treatment.[54]

Brain Tumors (Table 3)

In brain tumors, tumor perfusion, angiogenesis, tumor grading, therapeutic response, and prognosis can be

Table 3 ASL for brain tumors

Evaluation	ASL findings	ASL technique	Gold standard	Ref no.
Tumor grade and/or differentiation	A strong positive correlation between TBF derived from ASL and histopathological vascular density.	Single-delay pCASL (3.0T)	Histological vascular density	57
	CBF is higher in high-grade tumors than that in low-grade tumors, and CBF is correlated with tumor microvascular density.	Single-delay pCASL (1.5T)	Histological vascular density	58
	DWI, ASL, and ^{18}F-DOPA PET provide useful complementary information for pediatric diffuse astrocytic tumor grading.	Signle-delay PASL (1.5T)	Histology	59
	• Combining ADC and CBF measurements can be correctly classified as either low- or high-grade tumors.	Single-delay pCASL (1.5T and 3.0T)	Histology	60
	• ADC and CBF of diffuse midline glioma were similar to those of low-grade tumors. • Max rTBF of high-grade tumors is significantly higher than that of low-grade tumors. • rTBF of posterior fossa medulloblastoma is significantly higher than that of posterior fossa pilocytic astrocytoma.	Single-delay pCASL (3.0T)	Histology	61
	rCBF measured by ASL is significantly higher for choroid plexus carcinomas than that for choroid plexus papillomas.	Single-delay pCASL (1.5T)	Histology	62
Outcome prediction	Combining ADC, ASL, and ^{18}F-DOPA provides the high predictive power for prognosticating tumor progression.	Single-delay PASL (1.5T)	PFS	59
Tumor vascularity	Feeding vessels of meningiomas are reliably predicted by ss-pCASL.	Single-delay ss-pCASL (3.0T)	DSA	63
Differentiation between recurrence and treatment-related changes	ASL is superior to DSC for differentiation predominant recurrent high-grade glioma from radiation necrosis.	Single-delay pCASL (3.0T)	histology or clinical follow-up	66
	pCASL and DSC have nearly equivalent performance for the differentiation of progressive disease from pseudoprogression in adult patients with glioblastoma.	Single-delay pCASL (3.0T)	mRANO criteria and clinical follow-up	67

max rTBF, maximal relative tumor blood flow; mRANO, modified Response Assessment in Neuro-Oncology; PFS, progression-free survival; ss-pCASL, super-selective pseudo-continuous arterial spin labeling; TBF, tumor blood flow.

assessed using perfusion MR imaging. Dynamic susceptibility contrast (DSC) imaging has been widely used; however, it requires injection of a GBCA via high-flow power injectors and intravenous cannulas, which is a technical challenge in pediatric patients. In contrast, ASL is of particular interest in cases in which gadolinium-based perfusion is contraindicated, such as allergy and renal failure. Furthermore, repeated administration of a GBCA may induce its deposition in the brain.[4,5] ASL can provide perfusion information of brain tumors without GBCA injection. Moreover, there is no need for complicated leakage correction of GBCA algorithms to obtain CBF in ASL. Much of the previous perfusion MR studies using DSC focused on relative cerebral blood volume (CBV) changes, because the DSC measurement of CBV is simpler than that of CBF. Eliminating intra-arterial signals from total ASL signals using vascular suppression enables the measurement of arterial cerebral blood volume. There have been some papers focusing on the measurement of CBV with ASL; however, clinically available methods have not yet been established.[55,56] Therefore, CBF is used instead of relative CVB in clinical practice (Fig. 6).

ASL-based studies have shown promising results for the assessment of pediatric brain tumors, including stratification of malignant and/or high-grade brain tumors, outcome prediction, and vascularity.[57–63] Kikuchi et al. compared the tumor blood flow derived from ASL and the histopathological vascular density in pediatric brain tumors and found that the histopathological vascular density had a significant positive correlation with tumor blood flow, which correlated with the

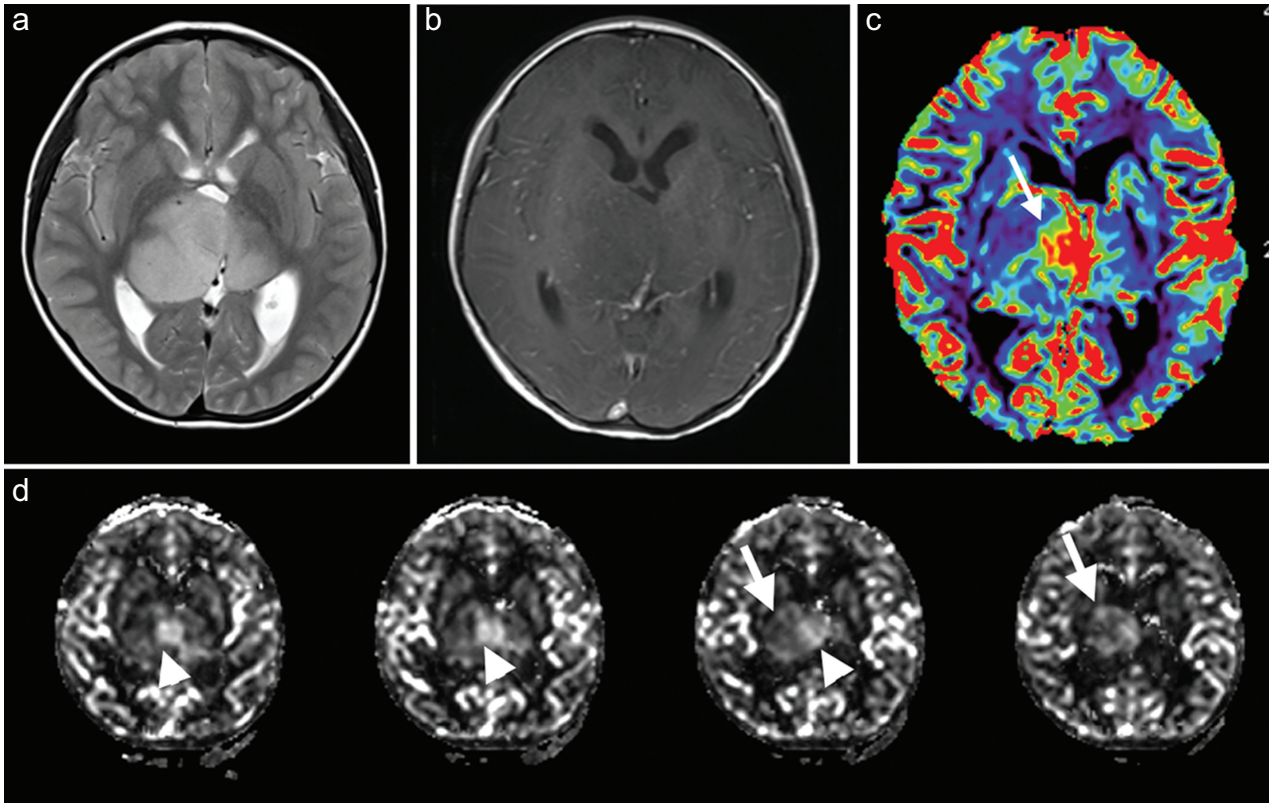

Fig. 6 A 7-year-old boy with thalamic glioma exhibiting high signal intensity on T2WI (**a**). There is no enhancement on post-contrast T1WI (**b**); however, on a DSC-CBV map (**c**), CBV increases within the tumor (arrow). On ASL-CBF maps (**d**), CBF of the tumor increases (arrows), and a remarkable increase of CBF (arrowheads) is observed at the area where CBV increases. ASL, arterial spin labeling; CBF, cerebral blood flow; CBV, cerebral blood volume; DSC, dynamic susceptibility contrast; T1WI, T1-weighted image; T2WI, T2-weighted image.

tumor grade.[57] Dangouloff-Ros et al. evaluated ASL-derived CBF in 129 pediatric patients with brain tumors for differentiating low- from high-grade neoplasms and assessing the correlation between CBF and the quantitative histological microvascular density.[58] They found that the cutoff value determined according to the tumor location yielded a high accuracy for differentiation, with more than 88% in 1.5-T MRI and 77% in 3.0-T MRI, and CBF was strongly correlated with the microvascular density.[58] A meta-analysis demonstrated that ASL-derived CBF measures showed a high diagnostic accuracy for discriminating low- from high-grade tumors in pediatric patients.[64] Further, the relative CBF, defined as the ratio of signal intensity in the lesion to that in the contralateral normal-appearing cortical gray matter, showed less variation among studies than did the absolute CBF.[64] Combining CBF derived from ASL and other image information including ADC and ^{18}F-DOPA PET has a high diagnostic power for differentiation between low- and high-grade pediatric brain tumors or for prognosticating tumor progression.[59,60] ASL and DSC are useful to evaluate tumor perfusion; however, Vidyasagar et al. reported the different sensitivity for physiology of tumor tissues between ASL and DSC: ASL provided comparable information to DSC in healthy tissues, but no significant correlations existed between DSC and ASL measures in the tumor region.[65]

Regarding the difference of CBF depending on each tumor pathology, Yeom et al. evaluated the ASL-derived relative tumor blood flow in various pathologic types of pediatric brain tumors and reported that it did not distinguish individual histology in their cohort, but it was significantly higher for medulloblastoma compared with pilocytic astrocytoma among posterior fossa tumors.[61] For diffuse midline glioma, ADC and CBF were similar to those of low-grade tumors.[60] For choroid plexus carcinomas, relative CBF was significantly higher than that of choroid plexus papillomas.[62]

Differentiation between tumor recurrence and treatment-related changes using MRI is challenging. In adult cases, combined analysis of CBF derived from ASL and ^{18}F-DOPA-PET uptake achieves high diagnostic performance in differentiating between progression and pseudo-progression in treated gliomas.[66]Also, ASL and DSC perfusion have nearly equivalent performance for the differentiation of progressive disease from pseudoprogression in adult patients with glioblastoma.[67]

ASL is also beneficial for the evaluation of hypervascular brain tumors, such as meningioma and hemangioblastoma.

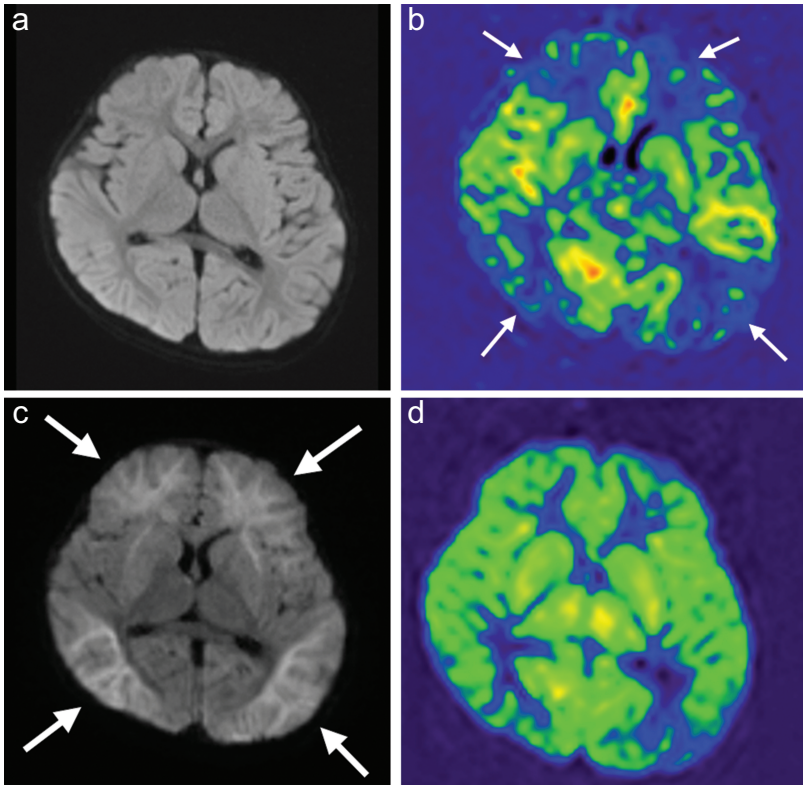

Fig. 7 An 11-month-old girl with AESD. An axial DWI 19 hours after early seizure (**a**) shows normal finding, but an ASL perfusion image (**b**) shows severe hypoperfusion in the bilateral frontal and parietal cortex (arrows). An axial DWI 1.5 hours after late seizure (**c**) shows hyperintensity in the bilateral cerebral subcortical white matter (BTA, arrows). The distribution of BTA is consistent with the area exhibiting hypoperfusion on ASL after early seizure. An ASL perfusion image 4 days after late seizure (**d**) shows mild hypoperfusion in the bilateral parietal lobes. AESD, acute encephalopathy with biphasic seizure and late reduced diffusion; ASL, arterial spin labeling; BTA, bright tree appearance; DWI, diffusion-weighted image.

In particular, for the pre-treatment assessment of tumor vascularity and the feeding arteries, ASL may assist in selecting potential candidates for preoperative DSA and embolization in clinical practice, which may reduce radiation exposure.[63]

Acute Encephalopathy with Biphasic Seizure and Late Reduces Diffusion: AESD

Acute encephalopathy with biphasic seizure and late reduced diffusion (AESD) is the major etiology of acute infectious encephalopathy in Japanese children (approximately 200 patients per year), and the most common causative pathogen of AESD was human herpesvirus 6.[68] AESD is clinically characterized by biphasic seizures and characteristic diffusion-weighted image (DWI) findings. Typically, a prolonged febrile seizure (early seizure) appears on day 1, followed by a cluster of complex partial seizures (late seizures) on days 4–6. Reduced diffusion in the subcortical white matter (so-called the bright tree appearance [BTA]) appears on days 3–9.[69]

Excitotoxic injury with delayed (or apoptotic) neuronal death is hypothesized to be a possible pathomechanism of AESD.[68] Takanashi et al. suggested that excitotoxic injury that induces an increase of glutamate concentrations during early seizures contributes to the pathomechanism of AESD based on MRS findings.[68] They also evaluated a postmortem case of AESD and compared its pathological findings with MR findings.[70] In pathological specimens, reduction of myelinated axons with early stage of astrocytosis at the corticomedullary junction in the absence of neuronal loss and an increased number of gemistocytic astrocytes at the corticomedullary junction were observed. These pathological changes may cause the development of BTA.

CBF change in AESD has been reported in several cases.[71–73] Cerebral perfusion on ASL changed over time in patients who underwent follow-up ASL, and various perfusions were noted more than 3 days after late seizures. Several case reports of AESD showed the perfusion change observed on ASL: a shift from hypoperfusion at approximately 20 hours after early seizures to hyperperfusion several days after late seizures.[71,72] In contrast, Yamanouchi et al. reported hypoperfusion in the subacute phase or later on SPECT.[74] Uetani et al. evaluated the time course of cerebral perfusion in 20 patients with AESD, and ASL showed hypoperfusion from 8.5 to

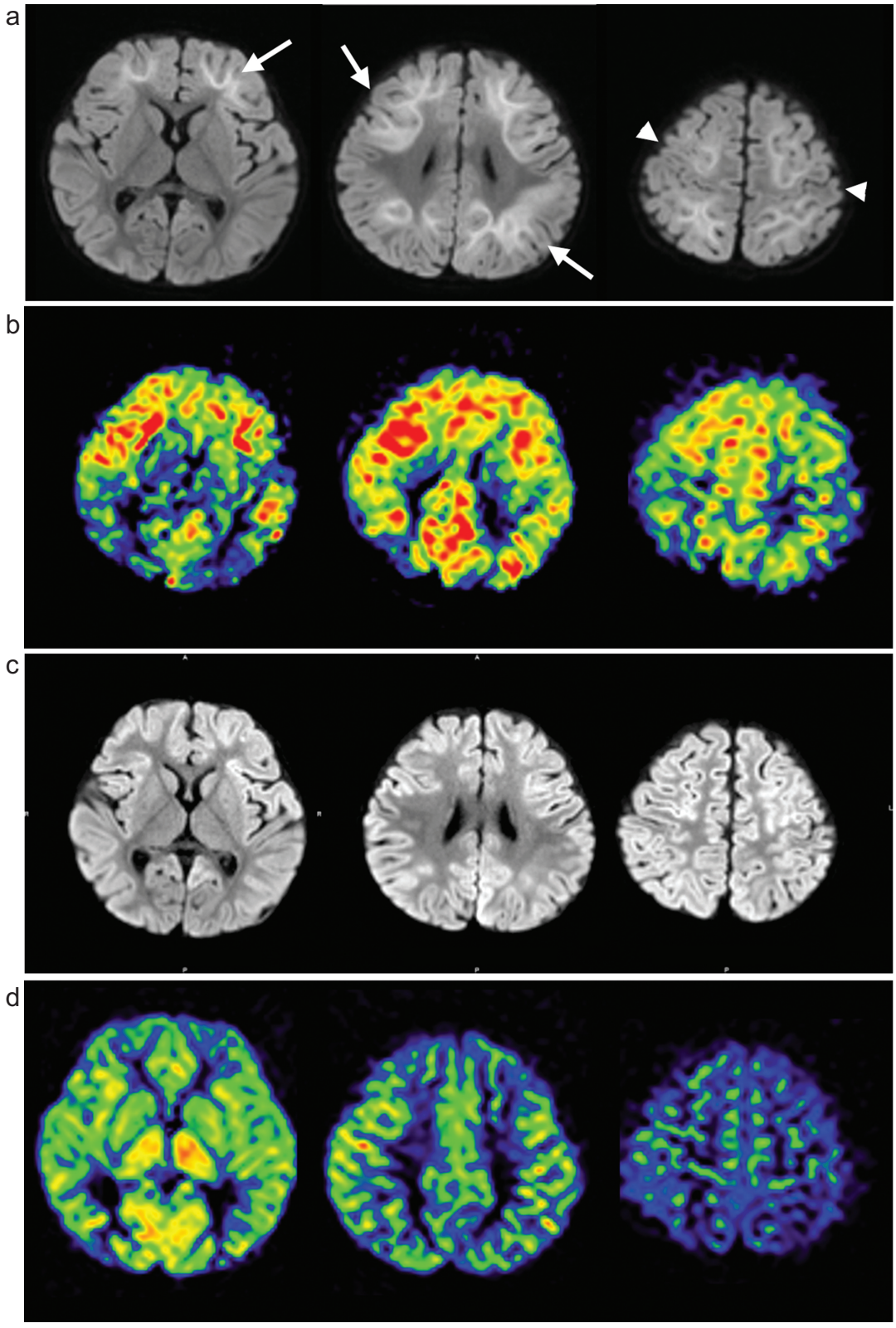

Fig. 8 A 15-month-old boy with AESD. Axial DWIs (**a**) 1.5 hours after late seizure show hyperintensity in the bilateral cerebral subcortical white matter (BTA, arrows), with a spared central sulcus area (arrowheads). ASL perfusion images show the hyperperfusion in bilateral frontal lobe and the left parietal lobe (**b**) 1.5 hours after late seizure. Axial DWIs (**c**) and ASL perfusion images (**d**) 3 days after late seizure show the disappearance of BTA and recovery of the perfusion abnormality. AESD, acute encephalopathy with biphasic seizure and late reduced diffusion; ASL, arterial spin labeling; BTA, bright tree appearance; DWI, diffusion-weighted image.

22 hours after early seizures and hyperperfusion within 24 hours after late seizures (Figs. 7 and 8).[73] Various perfusions were found later than 3 days after early seizures, including equivalent or decreased perfusion compared with that of normal brain perfusion regions. In addition, the distribution of perfusion abnormalities was consistent with that of BTA (Fig. 7).

The pathomechanism of decreased perfusion around early seizures has not been clarified; however, previous studies have suggested that post-ictal hypoperfusion at approximately 60–90 mins following seizures and vasoconstriction with glutamate, cyclooxygenase-2, and L-type calcium channels may contribute to perfusion abnormality and the BTA in AESD.[75,76] Therefore, hypoperfusion from 8.5 to 22 hours after early seizures might reflect postictal hypoperfusion and predict later development of AESD.[73]

Clinically, differentiation of AESD from the febrile seizure which is the common neurological disorder in infants and young children is difficult during early seizures. Differentiation between these two diseases is important, because the outcomes after prolonged febrile seizures are usually good, but mental deficits and/or epilepsy often remain in AESD. In addition, no useful imaging biomarkers for AESD have been identified. Therefore, the ASL findings in early seizures can improve the discrimination between AESD and prolonged febrile seizures. The timing from seizure cessation to MR examination and the distribution of hypoperfusion are very important in differentiating AESD from prolonged febrile seizures. Takanashi et al.[77] evaluated the prognostic value of MR spectroscopy in patients with acute excitotoxic encephalopathy and proposed that a decreased N-acetylaspartate (NAA) is the most effective metabolite for neurological prognosis prediction. The MR imaging information obtained from ASL and MR spectroscopy may have a useful prognostic value for AESD.

Migraine

The prevalence of migraine in the pediatric and adolescent populations has been reported to be 4.8% in Japanese junior high school students aged 12–15 years.[78] Approximately 30% of patients have migraine with aura.[78] Migraine aura is characterized by recurrent attacks of reversible neurological symptoms lasting between 5 and 60 minutes, with gradual spread over at least 5 minutes and accompanied by or followed within 60 minutes of headache.

The pathophysiology of migraine is still unclear; however, several theories, including vascular, cortical spreading depression (CSD), and trigeminal vascular theories have been proposed. In these theories, CSD plays an important role in the initiation of aura. It is characterized by a brief neuronal excitation, which initiates a depolarization wave that moves across the cortex at a rate of 3–5 mm/min, followed by prolonged inhibition of neuronal activity and

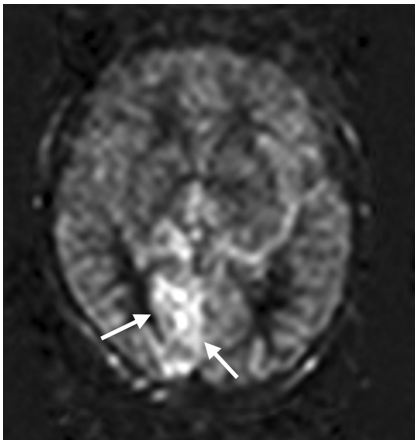

Fig. 9 A 14-year-old boy with migraine. Mild hyperperfusion in the right occipital lobe (arrows) is overserved on an ASL perfusion image 26 hours after disease onset. ASL, arterial spin labeling.

changes in vascular function. CSD is associated with significant vasoconstriction, and subsequent vasodilatation can start in the occipital cortex.[79]

Several ASL studies on migraine have been reported.[80–83] Cadiot et al.[80] reported that hypoperfusion was detected in 94% of patients with migraine with aura. Further, a shift of brain perfusion from hypoperfusion to hyperperfusion over time has been reported, and the time of the perfusion shift ranged from 6.7 to 17 hours.[81,82] Uetani et al.[83] evaluated brain perfusion in 49 pediatric and adolescent patients with migraine using ASL and reported that 11 of the patients (22%) exhibited perfusion abnormalities. Except for one patient with mild hyperperfusion, the remaining patients showed hypoperfusion predominantly in the occipital lobe (Figs. 9 and 10). The patients examined within 24 hours after onset showed hypoperfusion, whereas those examined 26 hours after onset showed hyperperfusion. All patients with perfusion abnormalities examined 4 days after onset showed normal perfusion. Occipital vulnerability is consistent with the pathophysiology of CSD, which is associated with the significant vasoconstriction followed by vasodilatation and could start in the occipital cortex; this finding is consistent with previous reports.[79,84] Furthermore, the presence of aura, motor disabilities, confusion, and hospitalization are related to abnormal perfusion.[83]

Hemiplegic migraine is a variant of migraine with aura, characterized by hemiplegia preceding headache. Attacks of hemiplegic migraine can manifest as acute neurological symptoms and signs. Thus, the differentiation between hemiplegic migraine and other diseases, such as acute brain infarction presenting hemiplegia, is important, because the treatment strategy depends on the underlying diseases. When the attack is over, the neurological deficit should resolve fully; however, residual neurological deficits may be observed. susceptibility-weighted imaging (SWI),

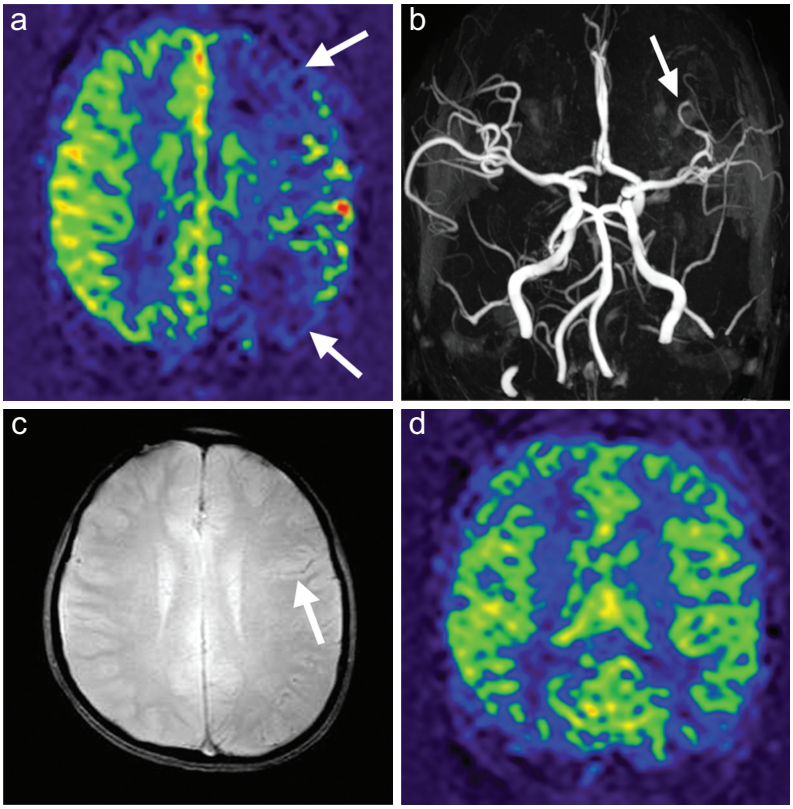

Fig. 10 An 11-year-old boy with hemiplegic migraine. Severe hypoperfusion in the left cerebral hemisphere (arrows) is observed on an ASL perfusion image (**a**) 7 hours after disease onset. Mild vasoconstriction in the left middle cerebral artery (**b**) is observed on a TOF-MRA (arrow). A prominent hypointense cortical vein (**c**) is observed on a T2*WI (arrow). The perfusion abnormality improves (**d**) 48 hours after disease onset. MRA, MR angiography; T2*WI, T2*-weighted image; TOF, time-of-flight.

T2*-weighted imaging (T2*WI), MRA, and ASL also provide useful information on brain perfusion in hemiplegic migraine (Fig. 10).[83] Each technique provided data supporting the following pattern: apparent constriction of the distal vessels on MRA and the presence of deoxygenated blood in the cerebral veins on SWI and T2*WI. Multimodal MR imaging sequences, including ASL, SWI, T2*WI, MRA, and DWI, distinguish hemiplegic migraine from stroke, with ASL being the most sensitive sequence to detect hemiplegic migraine.

Conclusion

ASL provides information on pediatric brain perfusion noninvasively. Knowledge of common artifacts and parameters affecting ASL findings is important when interpreting ASL images. ASL can help in the diagnosis and evaluation of vascular diseases and brain tumors, as well as the pathophysiology of AESD and migraine. ASL-based time-resolved MRA provides additional information on vascular diseases and may reduce the number of candidates for preoperative DSA with radiation exposure. ASL can be also used to assess the brain perfusion in a wide variety of pediatric neurological diseases, not discussed in this review, such as epilepsy, spectrum disorders, and mild traumatic brain injury.

Acknowledgments

The authors thank Yasuhiro Fujiwara (Department of Medical Imaging Sciences, Faculty of Life Sciences, Kumamoto University) for providing valuable suggestions on the ASL techniques and Prof. Akitake Mukasa (Department of Neurosurgery, Faculty of Life Sciences, Kumamoto University), Dr. Takeshi Sugahara (Department of Radiology, Kumamoto Red Cross Hospital), Yohei Kuroki (Department of Radiology, Kumamoto Red Cross Hospital), Dr. Yuichiro Muto (Department of Pediatrics, Kumamoto Red Cross Hospital), and Dr. Katsuki Hirai (Department of Pediatrics, Kumamoto Red Cross Hospital) for providing clinical images.

Conflicts of Interest

All authors declare that they have no conflicts of interest regarding this manuscript.

Supplementary Information

Supplementary files below are available online.

Supplementary Fig. 1a–1d

Whole brain ASL prefusion images at each PLD (200, 400, 600, 800, 1000, 1200, 1400, 1600, 1800, and 2000 ms) of Fig. 2. The ASL images were obtained using 3D-pCASL without vascular crusher, and the readout sequence was GRASE.

Supplementary Fig. 2a

Whole brain CBF map of Fig.2.

Supplementary Fig. 2b

Whole brain BAT map of Fig.2.

References

1. Haller S, Zaharchuk G, Thomas DL, Lovblad KO, Barkhof F, Golay X. Arterial spin labeling perfusion of the brain: emerging clinical applications. Radiology 2016; 281:337–356.
2. Williams DS, Detre JA, Leigh JS, Koretsky AP. Magnetic resonance imaging of perfusion using spin inversion of arterial water. Proc Natl Acad Sci USA 1992; 89:212–216.
3. Alsop DC, Detre JA. Reduced transit-time sensitivity in noninvasive magnetic resonance imaging of human cerebral blood flow. J Cereb Blood Flow Metab 1996; 16:1236–1249.
4. Kanda T, Ishii K, Kawaguchi H, Kitajima K, Takenaka D. High signal intensity in the dentate nucleus and globus pallidus on unenhanced T1-weighted MR images: relationship with increasing cumulative dose of a gadolinium-based contrast material. Radiology 2014; 270:834–841.
5. Flood TF, Stence NV, Maloney JA, Mirsky DM. Pediatric brain: repeated exposure to linear gadolinium-based contrast material is associated with increased signal intensity at unenhanced T1-weighted MR imaging. Radiology 2017; 282:222–228.
6. Hernandez-Garcia L, Lahiri A, Schollenberger J. Recent progress in ASL. Neuroimage 2019; 187:3–16.
7. Fujiwara Y, Ishida S, Kimura H. [6. Quantitative evaluation and problems for cerebral blood flow using arterial spin labeling (ASL)]. Nihon Hoshasen Gijutsu Gakkai Zasshi 2019; 75:1216–1222. (in Japanese)
8. van Osch MJ, Teeuwisse WM, Chen Z, Suzuki Y, Helle M, Schmid S. Advances in arterial spin labelling MRI methods for measuring perfusion and collateral flow. J Cereb Blood Flow Metab 2018; 38:1461–1480.
9. Togao O, Hiwatashi A, Obara M, et al. 4D ASL-based MR angiography for visualization of distal arteries and leptomeningeal collateral vessels in moyamoya disease: a comparison of techniques. Eur Radiol 2018; 28:4871–4881.
10. Tortora D, Scavetta C, Rebella G, et al. Spatial coefficient of variation applied to arterial spin labeling MRI may contribute to predict surgical revascularization outcomes in pediatric moyamoya vasculopathy. Neuroradiology 2020; 62:1003–1015.
11. Tortora D, Scavetta C, Rebella G, et al. Correction to: spatial coefficient of variation applied to arterial spin labeling MRI may contribute to predict surgical revascularization outcomes in pediatric moyamoya vasculopathy. Neuroradiology 2020; 62:1017.
12. Wang M, Yang Y, Wang Y, Li M, Zhang J, Zhang B. Vessel-selective 4D MRA based on ASL might potentially show better performance than 3D TOF MRA for treatment evaluation in patients with intra-extracranial bypass surgery: a prospective study. Eur Radiol 2021; 31:7214.
13. Suzuki Y, Fujima N, van Osch MJP. Intracranial 3D and 4D MR angiography using arterial spin labeling: technical considerations. Magn Reson Med Sci 2020; 19:294–309.
14. Togao O, Hiwatashi A, Obara M, et al. Acceleration-selective arterial spin-labeling MR angiography used to visualize distal cerebral arteries and collateral vessels in moyamoya disease. Radiology 2018; 286:611–621.
15. Hwang I, Cho WS, Yoo RE, et al. Revascularization evaluation in adult-onset moyamoya disease after bypass surgery: super-selective arterial spin labeling perfusion MRI compared with digital subtraction angiography. Radiology 2020; 297:630–637.
16. Togao O, Hiwatashi A, Yamashita K, et al. Acceleration-selective arterial spin labeling MR angiography for visualization of brain arteriovenous malformations. Neuroradiology 2019; 61:979–989.
17. Togao O, Obara M, Helle M, et al. Vessel-selective 4D-MR angiography using super-selective pseudo-continuous arterial spin labeling may be a useful tool for assessing brain AVM hemodynamics. Eur Radiol 2020; 30:6452–6463.
18. Alsop DC, Detre JA, Golay X, et al. Recommended implementation of arterial spin-labeled perfusion MRI for clinical applications: a consensus of the ISMRM perfusion study group and the European consortium for ASL in dementia. Magn Reson Med 2015; 73:102–116.
19. Dai W, Garcia D, de Bazelaire C, Alsop DC. Continuous flow-driven inversion for arterial spin labeling using pulsed radio frequency and gradient fields. Magn Reson Med 2008; 60:1488–1497.
20. Di Napoli A, Cheng SF, Gregson J, et al. Arterial spin labeling MRI in carotid stenosis: arterial transit artifacts may predict symptoms. Radiology 2020; 297:652–660.
21. Zaharchuk G, Do HM, Marks MP, Rosenberg J, Moseley ME, Steinberg GK. Arterial spin-labeling MRI can identify the presence and intensity of collateral perfusion in patients with moyamoya disease. Stroke 2011; 42:2485–2491.
22. Dai W, Shankaranarayanan A, Alsop DC. Volumetric measurement of perfusion and arterial transit delay using hadamard encoded continuous arterial spin labeling. Magn Reson Med 2013; 69:1014–1022.
23. Fan AP, Jahanian H, Holdsworth SJ, Zaharchuk G. Comparison of cerebral blood flow measurement with [^{15}O]-water positron emission tomography and arterial spin labeling magnetic resonance imaging: a systematic review. J Cereb Blood Flow Metab 2016; 36:842–861.
24. Ambarki K, Wåhlin A, Zarrinkoob L, et al. Accuracy of parenchymal cerebral blood flow measurements using pseudo-continuous arterial spin-labeling in healthy volunteers. AJNR Am J Neuroradiol 2015; 36:1816–1821.
25. Bambach S, Smith M, Morris PP, Campeau NG, Ho ML. Arterial spin labeling applications in pediatric and adult neurologic disorders. J Magn Reson Imaging 2022; 55:698–719.

26. Parkes LM, Rashid W, Chard DT, Tofts PS. Normal cerebral perfusion measurements using arterial spin labeling: reproducibility, stability, and age and gender effects. Magn Reson Med 2004; 51:736–743.
27. Jain V, Duda J, Avants B, et al. Longitudinal reproducibility and accuracy of pseudo-continuous arterial spin-labeled perfusion MR imaging in typically developing children. Radiology 2012; 263:527–536.
28. Forkert ND, Li MD, Lober RM, Yeom KW. Gray matter growth is accompanied by increasing blood flow and decreasing apparent diffusion coefficient during childhood. AJNR Am J Neuroradiol 2016; 37:1738–1744.
29. Wong AM, Liu HL, Tsai ML, et al. Arterial spin-labeling magnetic resonance imaging of brain maturation in early childhood: mathematical model fitting to assess age-dependent change of cerebral blood flow. Magn Reson Imaging 2019; 59:114–120.
30. Deibler AR, Pollock JM, Kraft RA, Tan H, Burdette JH, Maldjian JA. Arterial spin-labeling in routine clinical practice, part 1: technique and artifacts. AJNR Am J Neuroradiol 2008; 29:1228–1234.
31. Suzuki J, Takaku A. Cerebrovascular "moyamoya" disease. Disease showing abnormal net-like vessels in base of brain. Arch Neurol 1969; 20:288–299.
32. Donahue MJ, Dlamini N, Bhatia A, Jordan LC. Neuroimaging advances in pediatric stroke. Stroke 2019; 50:240–248.
33. Fan AP, Khalighi MM, Guo J, et al. Identifying hypoperfusion in moyamoya disease with arterial spin labeling and an [^{15}O]-water positron emission tomography/magnetic resonance imaging normative database. Stroke 2019; 50:373–380.
34. Fahlström M, Lewén A, Enblad P, Larsson EM, Wikström J. High intravascular signal arterial transit time artifacts have negligible effects on cerebral blood flow and cerebrovascular reserve capacity measurement using single postlabel delay arterial spin-labeling in patients with moyamoya disease. AJNR Am J Neuroradiol 2020; 41:430–436.
35. Qiu D, Straka M, Zun Z, Bammer R, Moseley ME, Zaharchuk G. CBF measurements using multidelay pseudocontinuous and velocity-selective arterial spin labeling in patients with long arterial transit delays: comparison with xenon CT CBF. J Magn Reson Imaging 2012; 36:110–119.
36. Hara S, Tanaka Y, Ueda Y, et al. Detection of hemodynamic impairment on ^{15}O gas PET using visual assessment of arterial spin-labeling MR imaging in patients with moyamoya disease. J Clin Neurosci 2020; 72:258–263.
37. Yun TJ, Paeng JC, Sohn CH, et al. Monitoring cerebrovascular reactivity through the use of arterial spin labeling in patients with moyamoya disease. Radiology 2016; 278:205–213.
38. Lee S, Yun TJ, Yoo RE, et al. Monitoring cerebral perfusion changes after revascularization in patients with moyamoya disease by using arterial spin-labeling MR imaging. Radiology 2018; 288:565–572.
39. Agarwal V, Singh P, Ahuja CK, Gupta SK, Aggarwal A, Narayanan R. Non-invasive assessment of cerebral microvascular changes for predicting postoperative cerebral hyperperfusion after surgical revascularisation for moyamoya disease: an arterial spin labelling MRI study. Neuroradiology 2021; 63:563–572.
40. El-Ghanem M, Kass-Hout T, Kass-Hout O, et al. Arteriovenous malformations in the pediatric population: review of the existing literature. Interv Neurol 2016; 5:218–225.
41. Le TT, Fischbein NJ, André JB, Wijman C, Rosenberg J, Zaharchuk G. Identification of venous signal on arterial spin labeling improves diagnosis of dural arteriovenous fistulas and small arteriovenous malformations. AJNR Am J Neuroradiol 2012; 33:61–68.
42. Fiehler J, Illies T, Piening M, et al. Territorial and microvascular perfusion impairment in brain arteriovenous malformations. AJNR Am J Neuroradiol 2009; 30:356–361.
43. Di Rocco C, Tamburrini G, Rollo M. Cerebral arteriovenous malformations in children. Acta Neurochir (Wien) 2000; 142:145–156; discussion 156–158.
44. Bednarz G, Downes B, Werner-Wasik M, Rosenwasser RH. Combining stereotactic angiography and 3D time-of-flight magnetic resonance angiography in treatment planning for arteriovenous malformation radiosurgery. Int J Radiat Oncol Biol Phys 2000; 46:1149–1154.
45. Aoyama H, Shirato H, Katoh N, et al. Comparison of imaging modalities for the accurate delineation of arteriovenous malformation, with reference to stereotactic radiosurgery. Int J Radiat Oncol Biol Phys 2005; 62:1232–1238.
46. Buis DR, Lagerwaard FJ, Dirven CM, et al. Delineation of brain AVMs on MR-angiography for the purpose of stereotactic radiosurgery. Int J Radiat Oncol Biol Phys 2007; 67:308–316.
47. Sunwoo L, Sohn CH, Lee JY, et al. Evaluation of the degree of arteriovenous shunting in intracranial arteriovenous malformations using pseudo-continuous arterial spin labeling magnetic resonance imaging. Neuroradiology 2015; 57:775–782.
48. Ozyurt O, Dincer A, Erdem Yildiz M, et al. Integration of arterial spin labeling into stereotactic radiosurgery planning of cerebral arteriovenous malformations. J Magn Reson Imaging 2017; 46:1718–1727.
49. Börcek A, Çeltikçi E, Aksoğan Y, Rousseau MJ. Clinical outcomes of stereotactic radiosurgery for cerebral arteriovenous malformations in pediatric patients: systematic review and meta-analysis. Neurosurgery 2019; 85:E629–E640.
50. Pollock JM, Whitlow CT, Simonds J, et al. Response of arteriovenous malformations to gamma knife therapy evaluated with pulsed arterial spin-labeling MRI perfusion. AJR Am J Roentgenol 2011; 196:15–22.
51. Blauwblomme T, Naggara O, Brunelle F, et al. Arterial spin labeling magnetic resonance imaging: toward noninvasive diagnosis and follow-up of pediatric brain arteriovenous malformations. J Neurosurg Pediatr 2015; 15:451–458.
52. Kodera T, Arai Y, Arishima H, et al. Evaluation of obliteration of arteriovenous malformations after stereotactic radiosurgery with arterial spin labeling MR imaging. Br J Neurosurg 2017; 31:641–647.
53. Leclerc X, Guillaud O, Reyns N, et al. Follow-up MRI for small brain AVMs treated by radiosurgery: is gadolinium really necessary?. AJNR Am J Neuroradiol 2020; 41:437–445.
54. Heit JJ, Thakur NH, Iv M, et al. Arterial-spin labeling MRI identifies residual cerebral arteriovenous malformation

following stereotactic radiosurgery treatment. J Neuroradiol 2020; 47:13–19.
55. Ishida S, Kimura H, Takei N, et al. Separating spin compartments in arterial spin labeling using delays alternating with nutation for tailored excitation (DANTE) pulse: a validation study using T_2 -relaxometry and application to arterial cerebral blood volume imaging. Magn Reson Med 2022; 87:1329–1345.
56. Petersen ET, Mouridsen K, Golay X. The QUASAR reproducibility study, Part II: results from a multi-center arterial spin labeling test-retest study. Neuroimage 2010; 49:104–113.
57. Kikuchi K, Hiwatashi A, Togao O, et al. Correlation between arterial spin-labeling perfusion and histopathological vascular density of pediatric intracranial tumors. J Neurooncol 2017; 135:561–569.
58. Dangouloff-Ros V, Deroulers C, Foissac F, et al. Arterial spin labeling to predict brain tumor grading in children: correlations between histopathologic vascular density and perfusion MR imaging. Radiology 2016; 281:553–566.
59. Morana G, Piccardo A, Tortora D, et al. Grading and outcome prediction of pediatric diffuse astrocytic tumors with diffusion and arterial spin labeling perfusion MRI in comparison with 18F-DOPA PET. Eur J Nucl Med Mol Imaging 2017; 44:2084–2093.
60. Hales PW, d'Arco F, Cooper J, et al. Arterial spin labelling and diffusion-weighted imaging in paediatric brain tumours. Neuroimage Clin 2019; 22:101696.
61. Yeom KW, Mitchell LA, Lober RM, et al. Arterial spin-labeled perfusion of pediatric brain tumors. AJNR Am J Neuroradiol 2014; 35:395–401.
62. Dangouloff-Ros V, Grevent D, Pagès M, et al. Choroid plexus neoplasms: toward a distinction between carcinoma and papilloma using arterial spin-labeling. AJNR Am J Neuroradiol 2015; 36:1786–1790.
63. Yoo DH, Sohn CH, Cho YD, et al. Superselective pseudocontinuous arterial spin labeling in patients with meningioma: utility in prediction of feeding arteries and preoperative embolization feasibility. J Neurosurg 2020; 135:1–7.
64. Delgado AF, De Luca F, Hanagandi P, van Westen D, Delgado AF. Arterial spin-labeling in children with brain tumor: a meta-analysis. AJNR Am J Neuroradiol 2018; 39:1536–1542.
65. Vidyasagar R, Abernethy L, Pizer B, Avula S, Parkes LM. Quantitative measurement of blood flow in paediatric brain tumours-a comparative study of dynamic susceptibility contrast and multi time-point arterial spin labelled MRI. Br J Radiol 2016; 89:20150624.
66. Pellerin A, Khalifé M, Sanson M, et al. Simultaneously acquired PET and ASL imaging biomarkers may be helpful in differentiating progression from pseudo-progression in treated gliomas. Eur Radiol 2021; 31:7395–7405.
67. Manning P, Daghighi S, Rajaratnam MK, et al. Differentiation of progressive disease from pseudoprogression using 3D PCASL and DSC perfusion MRI in patients with glioblastoma. J Neurooncol 2020; 147:681–690.
68. Takanashi J, Mizuguchi M, Terai M, Barkovich AJ. Disrupted glutamate-glutamine cycle in acute encephalopathy with biphasic seizures and late reduced diffusion. Neuroradiology 2015; 57:1163–1168.
69. Takanashi J, Oba H, Barkovich AJ, et al. Diffusion MRI abnormalities after prolonged febrile seizures with encephalopathy. Neurology 2006; 66:1304–1309;discussion 291.
70. Takanashi JI, Yasukawa K, Murofushi Y, Masunaga A, Sakuma H, Hayashi M. Loss of myelinated axons and astrocytosis in an autopsy case of acute encephalopathy with biphasic seizures and late reduced diffusion. Brain Dev 2018; 40:947–951.
71. Kuya K, Fujii S, Miyoshi F, et al. A case of acute encephalopathy with biphasic seizures and late reduced diffusion: Utility of arterial spin labeling sequence. Brain Dev 2017; 39:84–88.
72. Yokoyama H, Baba S, Oyama J, Moriyama K, Morio T. Early hypoperfusion on arterial spin labeling may be a diagnostic marker for acute encephalopathy with biphasic seizures and late reduced diffusion. Brain Dev 2017; 39:722.
73. Uetani H, Kitajima M, Sugahara T, et al. Perfusion abnormality on three-dimensional arterial spin labeling in patients with acute encephalopathy with biphasic seizures and late reduced diffusion. J Neurol Sci 2020; 408:116558.
74. Yamanouchi H, Mizuguchi M. Acute infantile encephalopathy predominantly affecting the frontal lobes (AIEF): a novel clinical category and its tentative diagnostic criteria. Epilepsy Res 2006; 70(Suppl1):S263–S268.
75. Gaxiola-Valdez I, Singh S, Perera T, Sandy S, Li E, Federico P. Seizure onset zone localization using postictal hypoperfusion detected by arterial spin labelling MRI. Brain 2017; 140:2895–2911.
76. Farrell JS, Colangeli R, Wolff MD, et al. Postictal hypoperfusion/hypoxia provides the foundation for a unified theory of seizure-induced brain abnormalities and behavioral dysfunction. Epilepsia 2017; 58:1493–1501.
77. Takanashi JI, Murofushi Y, Hirai N, et al. Prognostic value of MR spectroscopy in patients with acute excitotoxic encephalopathy. J Neurol Sci 2020; 408:116636.
78. Ando N, Fujimoto S, Ishikawa T, et al. Prevalence and features of migraine in Japanese junior high school students aged 12-15 yr. Brain Dev 2007; 29:482–485.
79. Lauritzen M. Pathophysiology of the migraine aura. The spreading depression theory. Brain 1994; 117:199–210.
80. Cadiot D, Longuet R, Bruneau B, et al. Magnetic resonance imaging in children presenting migraine with aura: Association of hypoperfusion detected by arterial spin labelling and vasospasm on MR angiography findings. Cephalalgia 2018; 38:949–958.
81. Boulouis G, Shotar E, Dangouloff-Ros V, et al. Magnetic resonance imaging arterial-spin-labelling perfusion alterations in childhood migraine with atypical aura: a case-control study. Dev Med Child Neurol 2016; 58:965–969.
82. Cobb-Pitstick KM, Munjal N, Safier R, Cummings DD, Zuccoli G. Time course of cerebral perfusion changes in children with migraine with aura mimicking stroke. AJNR Am J Neuroradiol 2018; 39:1751–1755.
83. Uetani H, Kitajima M, Sugahara T, et al. Perfusion abnormality on three-dimensional arterial spin labeling with a 3T MR system in pediatric and adolescent patients with migraine. J Neurol Sci 2018; 395:41–46.
84. Denuelle M, Fabre N, Payoux P, Chollet F, Geraud G. Posterior cerebral hypoperfusion in migraine without aura. Cephalalgia 2008; 28:856–862.